Shape-Controlled Ni Supported GDC Catalyst and its Application in Direct Ethanol Solid Oxide Fuel Cells

ECS Transactions, 111 (6) 1463-1472 (2023)
10.1149/11106.1463ecst ©The Electrochemical Society

Shape-Controlled Ni Supported GDC Catalyst and Its Application in Direct Ethanol Solid Oxide Fuel Cells

M. Machado[a], L. N. Rodrigues[a], V. B. Vilela[a], A. S. Ferlauto[b], T. Moraes[a], and F. C. Fonseca[a]

[a] IPEN-CNEN, Nuclear and Energy Research Institute, 05508-000, São Paulo, SP, Brazil
[b] UFABC, Federal University of ABC, 09210-580, Santo André, SP, Brazil

Matching catalytic activity with the high temperature heat treatments required to process solid oxide fuel cells (SOFCs) can be a challenge. Shape control is an interesting strategy to stabilize the surface of nanoparticles during heat treatments. In this study, nickel-based catalysts supported on shape-controlled (nanorods and nanocubes) gadolinium-doped cerium oxide (GDC) were evaluated for direct ethanol SOFCs. The morphology of the support had a significant effect on the catalytic activity. It was shown that the Ni catalyst supported on the GDC nanorods maintained high catalytic activity after heat treatments for catalytic layer sintering. Such catalyst was applied as catalytic layer on a SOFC operating directly on anhydrous ethanol at 700 °C. The fuel cell operated for more than 100 h under 0.6 V displaying consistent performance with no indication of degradation from carbon deposition.

Introduction

One of the greatest advantages of an SOFC is its ability to operate with hydrocarbons as fuel, including bioethanol. The high operating temperature of an SOFC (<600 °C) favors the direct internal ethanol steam reforming reaction (DIR) (Equation 1). Yet, carbon will form on the surface of the anode if ethanol is directly fed into the SOFC, due to the high Ni content (>30 vol%) of the state-of-the-art Ni/YSZ anode (1–4). The formation of carbon deposits will lead to a fast degradation of the fuel cell performance. As a result, a strategy was proposed to add a catalytic functional layer on top of the SOFC anode to reform the fuel before it gets in contact with the anode layer (5–8). In this design the material for the catalyst can be optimized for the highest possible hydrogen conversion. Nevertheless, the catalytic material must be compatible with the other materials in the cell and be stable under the severe processing and operating conditions of an SOFC.

$$CH_3CH_2OH + 3H_2O \leftrightharpoons 6H_2 + 2CO_2 \quad [1]$$

It has been reported that supported noble-metal catalysts such as Ir and Rh exhibit the highest activity towards C-C bond cleavage with negligible coke formation (9–11). However, a transition metal catalyst is a more viable option for industrial-scale application than a noble metal. Low-cost catalysts, based on a support with a low Ni content, are

commonly used as they were shown as stable and to have a high activity for H_2 conversion for ethanol steam reforming (8,12,13).

Besides the metal component of the catalyst, the support can have an important role in improving ethanol steam reforming. The use of cerium oxide (CeO_2) as a support has shown to be effective in improving ethanol decomposition and inhibiting coking (11). CeO_2 has a high oxygen storage capacity (OSC) due to its double oxidation state, allowing ceria to release oxygen under reducing conditions and adsorb oxygen under oxidizing conditions. Doping ceria with a trivalent cation creates extrinsic charge compensation defects as oxygen vacancies increasing the mobility of the species (14–16).

Furthermore, the morphology of the catalyst support has been shown to have a role in the Ni dispersion. High metal dispersion is correlated with increased active sites for catalytic reaction (17,18). Moreover, in the case of ceria the oxygen vacancies are morphology dependent. It has been observed that morphologies such as nanosheets, nanorods and nanocubes have exposed planes {110} and {100} and those have higher OSC and higher coke resistance (19,20). Rodrigues et al. (21) synthesized Ni/$Ce_{0.9}Sm_{0.1}O_{2-\delta}$ nanowires with increased catalytic activity for ethanol conversion compared to a commercial catalyst with the same composition. The higher activity was attributed to the support's high surface area, which provided many nucleation sites for the Ni nanoparticles over the whole surface of the support. Moraes et al. (22) synthesized CeO_2 with different morphologies (nanocube, nanorod, flower-like, and random shaped) impregnated with Ni. They observed that the Ni had a smaller crystallite size, which favored ethanol decomposition on the ceria-based support with adjusted morphology over the one with random-shaped nanoparticles.

An important factor in evaluating a catalyst for an SOFC is to consider the temperature effect on the catalyst. Heat treatment is typically employed for the application of a catalyst directly in an SOFC. The application of the catalyst layer on a SOFC consists of preparing an ink of the catalyst material with organic additives (i.e., solvents, pore formers, terpineol, polymers). A high temperature (~800 °C) is usually needed for the removal of the organics and for the attachment of the catalytic layer on the anode (6,23–25). Furthermore, the reduction of the NiO of the anode is typically carried out at a high temperature (>750 °C) before the operation of the fuel cell (25,26). A high temperature heat treatment alters the microstructure of the material and is associated with particles coarsening and to a decrease in the surface area leading to reduced catalytic activity, hence a higher rate of carbon formation and faster deactivation of the cell.

In this present study Ni/GDC catalysts with nanorods and nanocubes morphologies were evaluated as catalytic material for ethanol steam reforming. Furthermore, these nanostructured catalysts were heat treated in conditions analogous to the typical conditions for catalytic layer processing and of operation of an SOFC. The suitability of those materials for application on an SOFC were established. The Ni/GDC-NRs were applied as a catalytic layer on a high-performance anode supported SOFC and the stability of the cell under ethanol was assessed.

Experimental

Synthesis and Characterization of Catalyst

The synthesis of $Ce_{0.9}Gd_{0.1}O_{2-\delta}$ nanorods (GDC-NR) and $Ce_{0.9}Gd_{0.1}O_{2-\delta}$ nanocubes (GDC-NC) was adapted from previously reported synthesis of ceria by the hydrothermal method (21,27,28). First, a 14 M aqueous sodium hydroxide solution (NaOH, 99%, Sigma-Aldrich) was transferred to a Teflon-lined stainless-steel autoclave. Then an aqueous 5 mL solution containing the cerium ($Ce(NO_3)_3 \cdot 6H_2O$, 99%, Sigma Aldrich) gadolinium nitrates ($Gd(NO_3)_3 \cdot 6H_2O$, 99.9%, Sigma Aldrich) was gradually added to the NaOH solution under constant magnetic stirring. The autoclave was placed in a furnace at 110 °C for 24 h to obtain GDC-NRs and at 180 °C for 24 h to obtain GDC-NCs. The products were washed by five cycles of centrifugation with water and two cycles with ethanol. Finally, the synthesized materials were dried at 120 °C for 2 h in air.

Ni/GDC catalysts were prepared by incipient wetness impregnation of the supports, GDC-NRs and GDC-NCs, with an aqueous solution of $Ni(NO_3)_2 \cdot 6H_2O$ in order to obtain 5 wt% Ni in both supports. The impregnation consisted of dissolving the $Ni(NO_3)_2 \cdot 6H_2O$ in an aqueous solution. A volume of the solution matching the pore volume of the support is then slowly added to the support powder, such that the metal ions are adsorbed by the GDC support. After impregnation, the samples were calcined at 450 °C for 2 h in air. Moreover, the 5Ni/GDC-NR and 5Ni/GDC-NC samples were heated to 800 °C for 1 h in air for evaluation of catalytic activity after the heat treatment.

X-ray diffraction analyses of the as-prepared powders and of the samples heated at 800 °C were performed using a Miniflex II model diffractometer with Cu-Kα radiation source (0.15406 nm) in the range of 20° to 90° 2θ. The average crystallite sizes (*D*) were calculated using Scherrer Equation (Eq. 2):

$$D = 0.9 * \lambda / (\beta * \cos(\theta)) \quad [2]$$

where λ is the electromagnetic radiation wavelength, β is the full width at half maximum of the diffraction peak, and θ is the diffraction angle. The average crystallite sizes were calculated from the (111), (200), and (220) reflections.

The TEM analyses were carried out by JEOL JEM 2100 transmission electron microscope operated at 200 kV with a high angle annular dark field detector. Samples for TEM were prepared by drop-casting an aqueous suspension of the materials over a carbon coated copper grid, followed by drying under ambient conditions.

The specific surface areas (SSA) of the samples were determined by nitrogen gas adsorption measurements (at −196 °C) (Micromeritics Gemini VII) according to the Brunauer-Emmett-Teller (BET) method. Before the analysis, all samples were degassed under vacuum at 300 °C for 18 h in Micromeritics VacPrep 061.

Ethanol steam reforming (ESR)

The steam reforming of ethanol (ESR) was performed in a fixed bed quartz tubular reactor packed with 20 mg at 600 °C. Prior to reaction, the as-prepared catalysts and heat-treated catalysts were reduced under pure hydrogen flow (1.8 $L \cdot h^{-1}$) for 1 h. A reduction temperature of 450 °C was used for the as-prepared catalyst and 800 °C for the heat-treated catalyst. Water and ethanol were fed into the reactor using a system with two saturators to obtain a H_2O/CH_3CH_2OH molar ratio of 3. Nitrogen was used as carrier gas at a total flow rate of 60 $ml \cdot min^{-1}$. The ethanol conversion ($X_{ethanol}$) and selectivity (S_{xl}) of the obtained products as a function of the reaction time were determined by (Eqs. 3 and 4). The reactants and the reaction products were analyzed by gas chromatography (Agilent 7890A), equipped with a thermal conductivity detector (TCD) and a flame ionization detector (FID) connected in series.

$$X_{ethanol} = ((n_{ethanol})_{fed} - (n_{ethanol})_{exit})) / (n_{ethanol})_{fed} * 100 \quad [3]$$

$$S_{xl} = (n_x)_{produced}/(n_{totall})_{produced}) * 100 \quad [4]$$

where $(n_x)_{produced}$ = moles of x produced (x = H_2, CO, CO_2, CH_4, acetaldehyde, or ethylene) and $(n_{total})_{produced}$ = moles of H_2 + moles of CO + moles of CO_2 + moles of CH_4 + moles of acetaldehyde + moles of ethylene (i.e., the moles of water produced are not included).

Fuel Cell Fabrication and Testing

To fabricate the catalytic layer for testing under ethanol a Ni/GDC-NR catalytic ink was prepared by mixing the catalyst with terpineol, ethanol and polyvinylpyrrolidone (PVP, Sigma Aldrich, Mw ~55000). The ink was deposited on the anode of an anode-supported button cell (Fuel Cell Materials) by the airbrush technique. Prior to the deposition of the catalytic layer Au was painted and a gold wire was fixed on the anode for current collection.

The electrochemical properties of the anode supported cell with the Ni/GDC-NR catalytic layer were tested in the open flange test set-up from Fiaxell SOFC Technologies™. The current was collected by gold wires connected to a gold mesh (37 mm diameter) in the air outlet and one on the fuel side. The durability test was carried at a 0. 6 V bias under the flow of hydrogen and ethanol. The data was collected by a Zahner IM6 electrochemical workstation.

Results and Discussion

Characterization and Performance of Catalysts

Figure 1 shows the XRD patterns of 5Ni/GDC-NC and 5Ni/GDC-NR as-prepared and after heat treatment at 800°C. All diffractograms exhibited the single-phase fluorite structure of ceria (ICDD 96-900-9009). The shifts in the diffraction peaks are equivalent to the solid solution of GDC. There is no evidence of peaks corresponding to NiO. The 5Ni/GDC-NC catalyst presents more intense diffraction lines than the 5Ni/GDC-NR before

heat treatment, showing that the nanostructured GDC support in the form of nanocubes has higher crystallinity. After the heat treatment, the diffraction lines of 5Ni/GDC-NC catalysts remain practically unchanged. On the other hand, the 5Ni/GDC-NR samples after the heat treatment at 800 °C exhibit more intense diffraction lines than the as-prepared sample, evidencing the effect of the heat treatment on the nanostructured powders. The average crystallite size was calculated for all the catalysts before and after heat treatment. The 5Ni/GDC-NC exhibited average crystallite sizes of 42 nm before and 43 nm after the heat treatment at 800 °C, whereas 5Ni/GDC-NR crystallite size increases from 9 nm to 15 nm after the heat treatment at 800 °C.

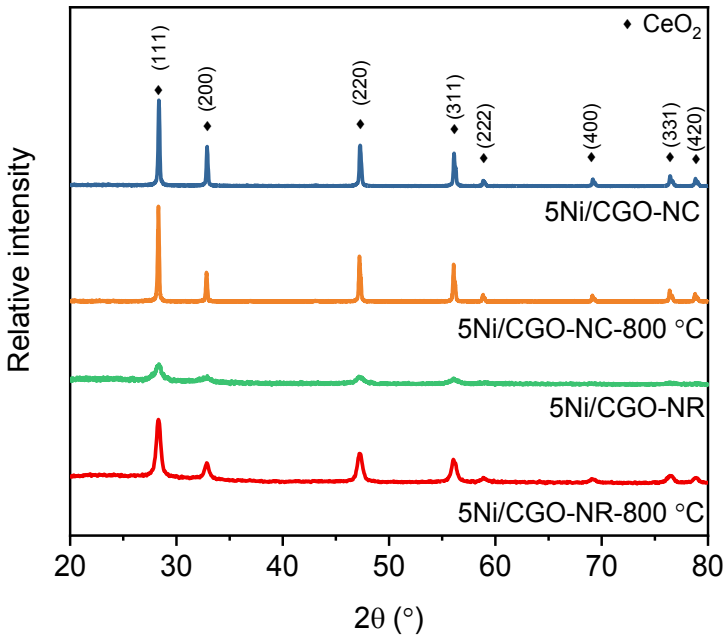

Figure 1. XRD patterns of 5Ni/GDC-NC and 5Ni/GDC-NR as-prepared and after the heat treatment at 800 °C.

The TEM image of the as-prepared 5Ni/GDC-NC (Figure 2a) shows a large size distribution, with the edges of the cubes having an estimated length of ~180 nm. The 5Ni/GDC-NR (Figure 2b) exhibit length of ~60 nm and a ~7 nm thickness. The dimensions of the NCs and NRs are compatible with the crystallite sizes calculated from the XRD (Figure 1).

The calculated specific BET surface area (SSA) evidences the effect of the heat treatment on the dimension of the particles. The 5Ni/GDC-NC exhibited a specific SSA = 2.7 $m^2 \cdot g^{-1}$ before and 2.0 $m^2 \cdot g^{-1}$ after the heat treatment at 800 °C, while 5Ni/GDC-NR have a considerably larger SSA both before (68.8 $m^2 \cdot g^{-1}$) and after (22.3 $m^2 \cdot g^{-1}$) the heat treatment. Interestingly, the surface area of the nanocubes (~2 $m^2 \cdot g^{-1}$) was practically unchanged while, the SSA of the 5Ni/GDC-NR displayed a three-fold decrease after treatment at 800 °C.

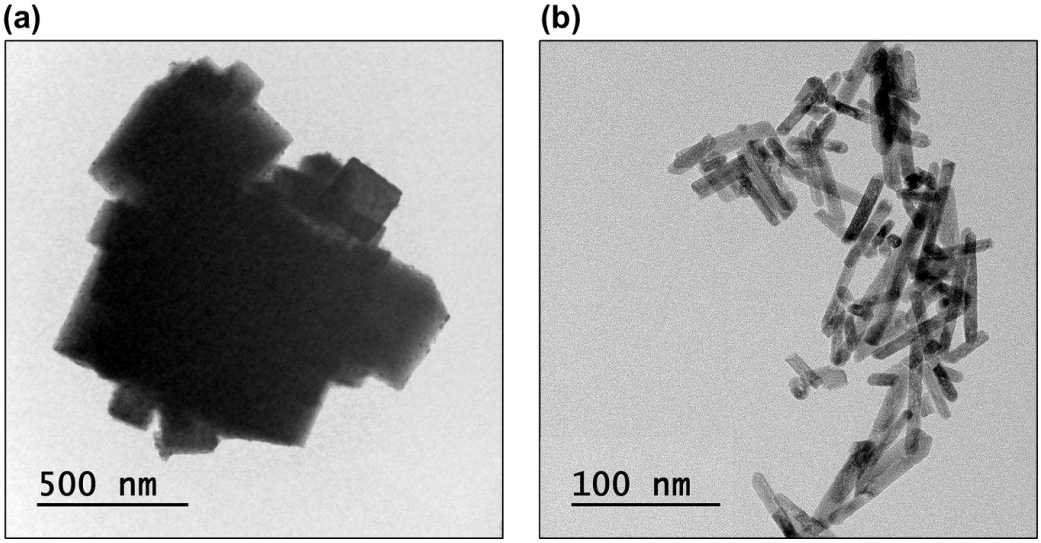

Figure 2. TEM images of the as-prepared catalyst: (a) 5Ni/GDC-NC and (b) 5Ni/GDC-NR.

The synthesized nanomaterials were studied for ethanol steam reforming (ESR). The ethanol conversion obtained for the ethanol steam reforming reactions at 600 °C with H_2O:EtOH = 3:1 (molar ratio) is shown in Figure 3. Both as-prepared catalysts showed 100% ethanol conversion during 25 h of reaction (Figure 3a and b). The 5Ni/GDC-NC catalyst heated at 800 °C showed an initial ethanol conversion of 97%, followed by a loss of activity reaction followed by a relatively stable conversion (~87%) with increasing reaction time. On the other hand, the 5Ni/GDC-NR catalyst heated at 800 ° showed 100% conversion of ethanol upon 15 h of reaction and a very small deactivation with increasing reaction time (~99% at 25 h).

The heat treatment at high temperatures changes the morphology and decreases the GDC support surface area, particularly the GDC-NR, and the coarsening of the Ni particles, resulting in fewer active sites for the catalytic reaction. The results shown in Figure 3 indicate that the 5Ni/GDC-NR remains active even after heat treatment at 800 °C, possibly due to higher surface area and therefore dispersion of Ni in the support. Although the 5Ni/GDC-NC catalyst's morphology and surface area do not significantly change after heat treatment at 800 °C, the initial relatively low specific surface area inhibits a high dispersion of Ni nanoparticles, which facilitates coarsening of the Ni particles upon heating.

Regarding the distribution of products, in Figure 3, all ESR show ~70% of selectivity to H_2 with rather stable distribution of products. The formation of H_2, CO, CO_2 and traces of CH_4, was detected in all catalysts (12). Besides the ethanol steam reforming (Eq. 1), several reactions can occur in parallel, such as: (i) the decomposition of ethanol (Eq. 5), (ii) the dehydrogenation of ethanol to acetaldehyde (Eq. 6), (iii) the steam reforming of acetaldehyde (Eq. 7) and (iv) the water gas shift reaction (Eq. 8). The results obtained for the catalysts suggest that the ethanol reforming, the dehydrogenation of ethanol to acetaldehyde followed by the steam reforming of acetaldehyde and the water gas shift reactions were favoured in these catalysts. The deactivation of the catalysts upon heat treatment was accompanied by the formation of acetaldehyde and a drop in H_2 selectivity. As the catalyst needs metallic sites to break the C-C bond, it is suggested that the catalyst

that exhibited deactivation and increasing acetaldehyde selectivity at the expense of H_2 were losing metallic active sites.

$$CH_3CH_2OH \rightleftharpoons CO + H_2 + CH_4 \quad [5]$$

$$C_2H_5OH \rightleftharpoons C_2H_4O + H_2 \quad [6]$$

$$C_2H_4O + H_2O \rightleftharpoons 2CO + 3H_2 \quad [7]$$

$$CO + H_2O \rightleftharpoons CO_2 + H_2 \quad [8]$$

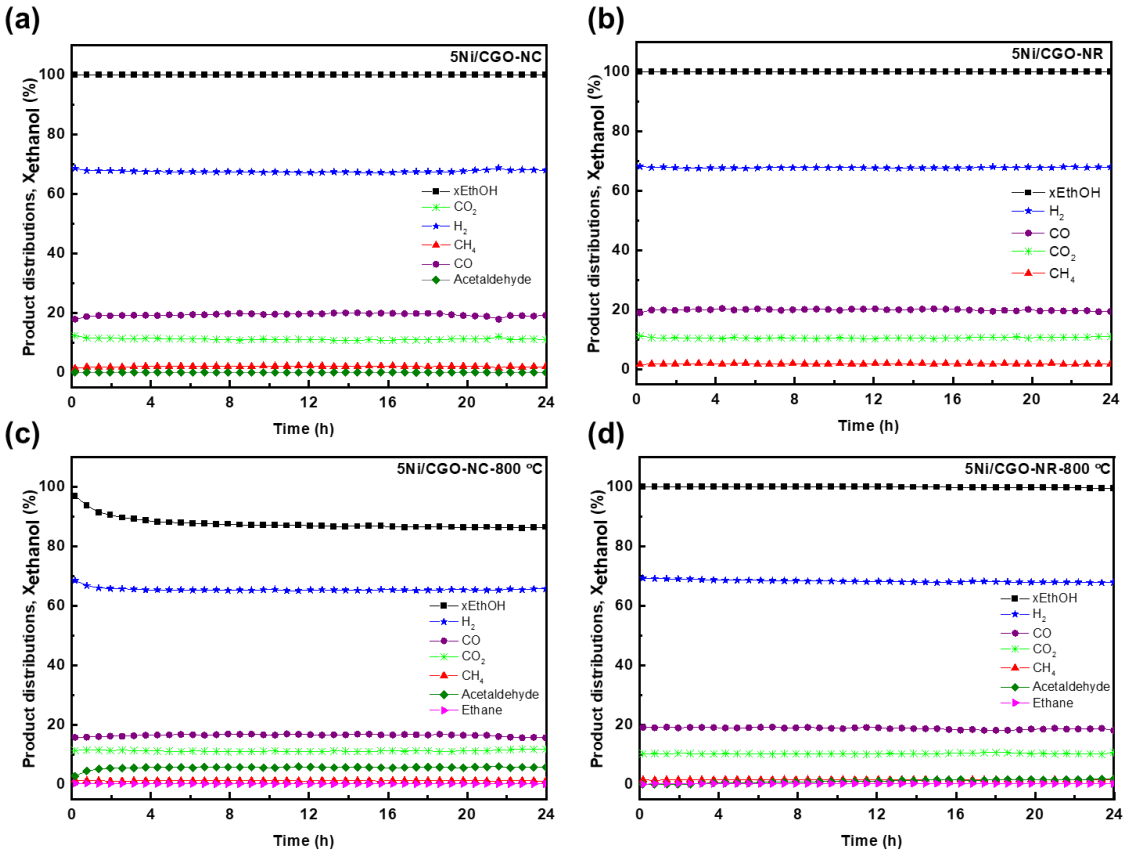

Figure 3. Ethanol conversion and product distribution obtained for the catalysts during ethanol steam reforming reactions at 600 °C and H_2O/ethanol molar ratio of 3, for (a) 5Ni/CGO-NC, (b) 5Ni/CGO-NR, (c) 5Ni/CGO-NC-800 °C, (d) 5Ni/CGO-NR-800 °C.

Fuel Cell Testing

The experimental results showed that the high SSA of GDC-NR promoted a high dispersion of Ni nanoparticles that contributed to a high catalytic activity at 600 °C towards ethanol steam reforming. Thus, the 5Ni/GDC-NR catalyst was chosen to be applied as a catalytic layer for the direct ethanol SOFC tests.

To investigate the effect of the catalytic layer on the electrochemical performance of the fuel cell directly fed with anhydrous ethanol, a short-term durability test was carried out for 110 h at 700 °C and 0.6 V (Figure 4). The test was run under flow of synthetic air on the cathode side, and at first hydrogen was used as a fuel and then it was changed to ethanol. The flow rates were calculated to carry an equivalent theoretical number of electrons to the anode. Thus, by considering Eq. 1, a 1/6 ratio between ethanol and H_2 was set while keeping a constant total flow rate of 6 $L \cdot h^{-1}$.

At the start of the experiment the current density of the cell at 0.6 V is at 1.02 $A \cdot cm^{-2}$. In the first 17 h under hydrogen the cell experienced a steep drop in current by rate of -21.6 $mA \cdot h^{-1}$, possibly related to the conditioning of the cell. By changing the fuel to ethanol there was a continuous decrease in the current density with time under a degradation rate of -3.96 $mA \cdot h^{-1}$. After 90 h under ethanol, the fuel cell stabilizes the current output to 0.27 $A \cdot cm^{-2}$ and remains stable for 20 h of operation with dry ethanol after which the fuel is changed back to ethanol and the current increases to 1.11 $A \cdot cm^{-2}$. Such a decrease in current output on ethanol is related to the complex reactions taking place at both the anode and catalytic layers. The Faradaic efficiency for ethanol is possibly lower than that of H_2, the larger molecule size of ethanol imposes restrictions to mas transport in the porous layers, moreover the catalytic conversion of ethanol to hydrogen is limited. Residence time is also a key parameter for the catalytic reaction. The higher the residence time, the higher the ethanol conversion and H_2 yield (29). A possible cause for the current increase when H_2 is flown is related to incomplete conversion of ethanol that may be associated with a lower residence time in the fuel cell test rig as compared to the fixed bed reactor for ESR.

It is interesting to note that the current density under H_2 at the beginning and at the end of the test is similar, indicating that the operation under ethanol promoted no additional degradation of the fuel cell's performance. Such an excellent result demonstrates that the active catalyst based on GDC-NR and Ni is capable of sustaining ethanol steam reforming at 700 °C, using the water produced through the catalytic reaction of the electrochemical oxidation of H_2.

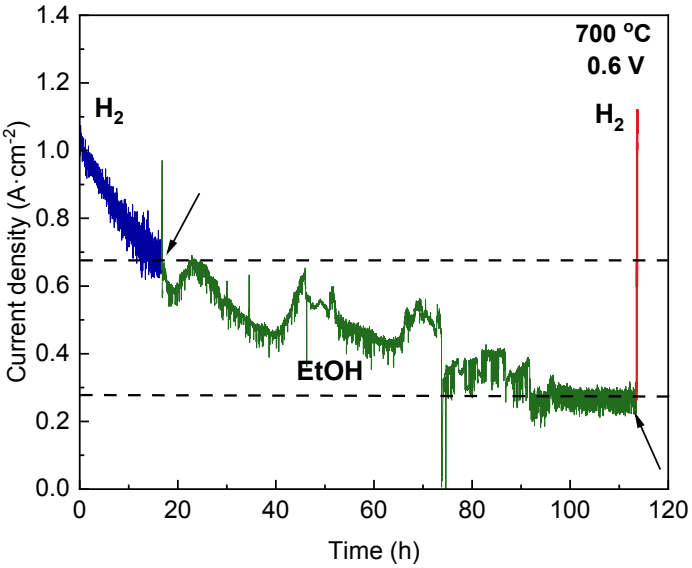

Figure 4. Durability test of the anode-supported single cell with the 5Ni/CGO-NR catalytic layer at 700 °C. The arrows indicate the beginning and end time for the operation under ethanol.

Conclusion

Ni-based catalysts supported on shape-controlled GDC nanoparticles showed excellent properties for the ethanol steam reforming at relatively low temperature (600 °C). The stability of the catalytic properties of such nanostructures were demonstrated after heat treatment compatible with the preparation of functional layers for solid oxide fuel cell applications. The morphology of the support was shown to have an important role in the conversion of ethanol. The anode supported fuel cell with Ni/CGO-NR catalytic layer exhibited a relatively stable performance of the during the continuous operation under dry ethanol at 700 °C. The experimental results indicate the promising strategy of using Ni-based catalytic layer for the direct ethanol operation of SOFC at intermediate temperatures.

Acknowledgments

Authors would like to acknowledge Brazilian agencies FAPESP grants n° 2019/15110-2, 2022/06295-1, and CNPq SisH2 n° 407967/2022-2. FCF and ASF are CNPq fellows.

References

1. S. M. de Lima, A. M. da Silva, L. O. O. da Costa, U. M. Graham, G. Jacobs, B. H. Davis, L. V. Mattos, and F. B. Noronha, *J. Catal.*, **268**(2), 268–281 (2009).
2. M. Compagnoni, A. Tripodi, A. Di Michele, P. Sassi, M. Signoretto, and I. Rossetti, *Int. J. Hydrog. Energy*, **42**(47), 28193–28213 (2017).
3. A. A. A. da Silva, N. Bion, F. Epron, S. Baraka, F. C. Fonseca, R. C. Rabelo-Neto, L. V. Mattos, and F. B. Noronha, *Appl. Catal. B*, **206**, 626–641 (2017).

4. B. Farrell and S. Linic, *Appl. Catal. B*, **183**, 386–393 (2016).
5. N. K. Monteiro, F. B. Noronha, L. O. O. da Costa, M. Linardi, and F. C. Fonseca, *Int. J. Hydrog. Energy*, **37**(12), 9816–9829 (2012).
6. M. C. Steil, S. D. Nobrega, S. Georges, P. Gelin, S. Uhlenbruck, and F. C. Fonseca, *Appl. Energy*, **199**, 180–186 (2017).
7. S. D. Nobrega, M. V. Galesco, K. Girona, D. Z. de Florio, M. C. Steil, S. Georges, and F. C. Fonseca, *J. Power Sources*, **213**, 156–159 (2012).
8. P. Zhang, Z. Yang, Y. Jin, C. Liu, Z. Lei, F. Chen, and S. Peng, *Int. J. Hydrog. Energy*, **46**(79), 39369–39386 (2021).
9. M. D. Zhurka, A. A. Lemonidou, and P. N. Kechagiopoulos, *Catal. Today*, **368**, 161–172 (2021).
10. T. Hou, B. Yu, S. Zhang, T. Xu, D. Wang, and W. Cai, *Catal. Commun.*, **58**, 137–140 (2015).
11. B. Zhang, X. Tang, Y. Li, W. Cai, Y. Xu, and W. Shen, *Catal. Commun.*, **7**(6), 367–372 (2006).
12. S. Ogo and Y. Sekine, *Fuel Process. Technol.*, **199**, 106238 (2020).
13. M. Greluk, W. Gac, M. Rotko, G. Słowik, and S. Turczyniak-Surdacka, *J. Catal.*, **393**, 159–178 (2021).
14. H. Inaba, *Solid State Ion.*, **83**(1–2), 1–16 (1996).
15. B. Steele, *Solid State Ion.*,**129**(1–4), 95–110 (2000).
16. G. R. Ferreira, F. G. E. Nogueira, A. F. Lucrédio, and E. M. Assaf, *Catal. Lett.*, (2022).
17. S. Yang, F. Zhou, Y. Liu, L. Zhang, Y. Chen, H. Wang, Y. Tian, C. Zhang, and D. Liu, *Int. J. Hydrog. Energy*, **44**(14), 7252–7261 (2019).
18. D. G. Araiza, A. Gómez-Cortés, and G. Díaz, *Catal Today*, **349**, 235–243 (2020).
19. X. Du, D. Zhang, L. Shi, R. Gao, and J. Zhang, *J Physl Chem C*, **116**(18), 10009–10016 (2012).
20. I. I. Soykal, B. Bayram, H. Sohn, P. Gawade, J. T. Miller, and U. S. Ozkan, *Appl. Cat A*, **449**, 47–58 (2012).
21. T. S. Rodrigues, A. B. L. de Moura, F. A. e Silva, E. G. Candido, A. G. M. da Silva, D. C. de Oliveira, J. Quiroz, P. H. C. Camargo, V. S. Bergamaschi, J. C. Ferreira, M. Linardi, and F. C. Fonseca, *Fuel*, **237**, 1244–1253 (2019).
22. T. S. Moraes, R. C. R. Neto, M. C. Ribeiro, L. V. Mattos, M. Kourtelesis, X. Verykios, and F. B. Noronha., *Top. Catal.*, **58**(4), 281–294 (2015).
23. S. D. Nobrega, P. Gelin, S. Georges, M. C. Steil, B. L. Augusto, F. B. Noronha, and F. C. Fonseca, *J. Electrochem. Soc.*, **161**(3), F354 (2014).
24. M. Liao, W. Wang, R. Ran, and Z. Shao, *J. Power Sources*, **196**(15), 6177–6185 (2011).
25. A. A. A. da Silva, M. C. Steil, F. N. Tabuti, R. C. Rabelo-Neto, F. B. Noronha, L. V. Mattos, and F. C. Fonseca, *Int. J. Hydrog. Energy*, **46**(5), 4309–4328 (2021).
26. S. Anelli, F. Baiutti, A. Hornés, L. Bernadet, M. Torrell, and A. Tarancó, *J. Mater. Chem.*, *A* **7**(48), 27458–27468 (2019).
27. H.-X. Mai, L.-D. Sun, Y.-W. Zhang, R. Si, W. Feng, H.-P. Zhang, H.-C. Liu, and C.-H. Yan, *J. Phys. Chem. B*, **109**(51), 24380–24385 (2005).
28. W. Shi, S. Song, and H. Zhang, *Chem. Soc. Rev.*, **42**(13), 5714 (2013).
29. L. V. Mattos and F. B. Noronha, *J. Catal.*, **233**(2), 453–463 (2005).